

Evaluation of the adsorption potential of Fe₃O₄ immobilized waste rock wool for the removal of Pb(II) from the aquatic environment

Da Zhao^a, Ping Sun^a, Dazhi Liu^a, Chunhao Liang^b, Chaoqun Zang^b, Haibo Long^{c,*}

^aKey Laboratory of Regional Environment and Eco-Remediation of Ministry of Education, College of Environment, Shenyang University, Shenyang, 110044, China, emails: zhaoda81@yeah.net (D. Zhao), 355119629@qq.com (P. Sun), 706343627@qq.com (D.Z. Liu)

^bLiaoning Academy of Agricultural Sciences, Shenyang, 110161, China, emails: 37216849@qq.com (C.H. Liang), 327494006@qq.com (C.Q. Zang)

^cCollege of Mechanical Engineering, Shenyang University, Shenyang 110044, China, Tel. +8618602424060; email: dragon_haibo@yeah.net

Received 17 July 2020; Accepted 21 January 2021

ABSTRACT

Rock wool (RW) is an inorganic fiber material with chemical stability and fire retardancy also available in low cost. RW is widely used in building exterior wall insulation and interior sound insulation and accounts for an increasing proportion of demolition waste from buildings. Iron oxide can efficiently remove pollutants from aqueous solution. In our research, Fe₃O₄ nanoparticles were deposited on acid-modified waste rock wool (ARW) with the coprecipitation method, and a novel adsorbent for lead was generated. Sorbent materials were characterized by scanning electron microscopy, energy dispersive X-ray spectroscopy, Fourier transform infrared spectroscopy and X-ray diffraction, and adsorption parameters under different reaction conditions (pH, concentration, contact time, and sorbent dosage) were investigated. The results indicate that the new adsorbent adsorbs lead more efficiently than Fe₃O₄ alone, because the incorporation of rock wool reduces the agglomeration effect. The adsorption of lead into Fe₃O₄ deposited acid-modified waste rock wool fiber (ARWF) obeys pseudo-second-order kinetics and Langmuir models. Batch adsorption experiments show that the ARWF can efficiently remove lead from water with a maximum adsorption capacity of 123.15 mg/g and can adsorb 99.45% of lead in 30 min when pH is 4–8. ARWF was also demonstrated to have good potential for regeneration and reuse after four consecutive cycles. These results suggest that waste rock wool loaded with Fe₃O₄ nanoparticles is a promising material for water treatment.

Keywords: Waste rock wool; Fe₃O₄; Pb(II); Adsorption

1. Introduction

Lead is a highly toxic metal that was frequently used throughout history. In nature, lead is characterized by wide distribution, ease of extraction, and ease of processing. Lead ions in water pose a serious environmental concern, which is mainly due to natural weathering and

the discharge of lead-containing effluents such as mine exploitation, petroleum refining, lead-acid battery production, and chemical reagents [1,2]. Lead in water is not biodegradable and undergoes bioaccumulation, meaning that it accumulates in the food cycle to have large potential negative impacts on humans [3]. Therefore, different authorities have specified thresholds for Pb(II) concentration allowed

* Corresponding author.

in drinking water. Various technologies have been developed to remove lead ions from effluents, including ion exchange technology [4], chemical precipitation method [5], membrane separation technology [6], and adsorption technology [7]. Of these, adsorption technology is beneficial due to its low cost, simple operation, and high efficiency as well as its lack of harm to organisms in the water environment and the wide availability of adsorption materials [8,9]. Conventional adsorbents, such as activated carbon, alumina, quartz sand, and zeolite, have complex regeneration processes and are costly and difficult to separate from water; thus, their widespread application is limited. Therefore, demands for inexpensive sorbents with high adsorption capacity are pressing [10–12]. With the development of nanotechnology, various novel nanosorbents have been created. Iron-based nanomaterials such as Fe_3O_4 are an area of great research interest due to their fast adsorption rate, high adsorption performance, easy separation and regeneration, economy, and high efficiency [13]. However, these tiny nanoparticles agglomerate easily and form large particle precipitation, which reduces adsorption efficiency. To solve these problems, there is a strong need for low-cost carrier materials with simple fabrication processes.

Rock wool (RW) is an inorganic fiber widely used in building exterior wall insulation, indoor sound insulation, fire prevention, cement reinforcement, pipeline insulation, and soilless culture. It is made of dolomite and basalt and has outstanding buffering capacity, excellent chemical stability, flame retardance, and low cost [14–16]. Much solid waste is generated each year due to building demolitions in China, and this causes severe environmental pollution and loss of resources. The world produces over 200 million tons of construction demolition waste each year, compromising 30%–40% of total urban solid waste [17]. Rock wool insulation materials are widely used in construction and infrastructure projects, accounting for a growing proportion of construction demolition waste. The majority of waste rock wool is discarded or buried, which causes severe environmental pollution due to lack of biodegradation. This is also a substantial waste of material and human resources [18,19]. Therefore, there is significant interest in recycling waste rock wool.

The objective of this research was to fabricate a neotype material on the basis of acid-modified waste rock wool fiber (ARWF) with iron oxide nanoparticles, and to use this material for the removal of Pb(II) from water. The morphological and physicochemical properties of iron oxide/acid-modified rock wool fiber (ARWF) were determined by scanning electron microscopy (SEM), energy dispersive X-ray spectroscopy (EDX), Fourier transforms infrared spectroscopy (FTIR) and X-ray diffraction (XRD). The impacts of pH, contact time, initial Pb(II) concentration, and adsorbent dosage on the removal efficiency and capacity were also investigated. The adsorption kinetic experiments were fitted with pseudo-first-order and pseudo-second-order models, and Langmuir and Freundlich models were employed to fit the adsorption equilibrium data. Under experimental conditions, the adsorption mechanism of ARWF on Pb(II) in aqueous solution was preliminarily determined. We expect that this research will inspire advances in wastewater purification and waste rock wool recycling.

2. Materials and methods

2.1. Materials

Waste rock wool (RW) was collected from abandoned exterior insulation materials (Shenyang, China). Analytical grade reagents, including $\text{Pb}(\text{NO}_3)_2$, $\text{FeSO}_4 \cdot 7\text{H}_2\text{O}$, HCl, $\text{FeCl}_3 \cdot 6\text{H}_2\text{O}$, HNO_3 , and NaOH, were purchased from Sinopharm Chemical Reagent Shenyang Co. Ltd. Lead solution ($2,000 \text{ mg L}^{-1}$) was prepared by dissolving $\text{Pb}(\text{NO}_3)_2$ in deionized water followed by serial dilution as required during use. All chemical solutions used in experiments were prepared in deionized water.

2.2. Sorbent preparation

The RW collected was washed repeatedly with deionized water, then dipped into HCl solution (1.0 M) at room temperature for 15 min, stirring continuously (120 rpm). The precipitates were collected using a strainer and cleaned with deionized water several times. The precipitates were subsequently dried in an oven for 12 h at 333 K and ground to obtain ARW.

The functional ARW was generated using the co-precipitation method [20]. First, $\text{FeCl}_3 \cdot 6\text{H}_2\text{O}$ and $\text{FeSO}_4 \cdot 7\text{H}_2\text{O}$ were immersed in deionized water (200 mL), keeping the molar ratio of Fe^{3+} to Fe^{2+} at 2:1. ARW (1 g) was then added and mixed evenly at room temperature. NaOH (10 M) was slowly added to the solution until the pH was 12. The solution was agitated vigorously for 2 h and then incubated for 24 h at room temperature. The precipitates were then collected by magnetic separation. After repeated cleaning, the collected precipitates were dried in an oven at 333 K for 12 h to obtain iron oxide supported ARWF. The mass ratios of ARW and Fe in ARWF composites were established on 4:1, 2:1, 1:1, and 0.5:1, respectively. The ARWF sample prepared was ground and sealed for preservation.

2.3. Characterization of samples

The microstructure and morphology of the ARWF materials were estimated on a scanning electron microscope (Hitachi S-4800, Tokyo, Japan). The chemical elemental distribution of the samples was characterized using EDX on SEM. The crystalline pattern of the materials was monitored using an X-ray diffractometer (Bruker D8, Brerica, Massachusetts, USA). The composition of the adsorbent was determined by comparison with the spectra in the JADE program. Active functional groups on the adsorbent's surface were also measured by FTIR spectroscopy (Varian FTIR3000, Palo Alto, California, USA).

2.4. Adsorption experiments

In this research, $\text{Pb}(\text{NO}_3)_2$ was chosen as the target pollutant. Pb(II) stock solutions were prepared by dissolving 3.197 g of $\text{Pb}(\text{NO}_3)_2$ in 1,000 mL of deionized water. The stock solution was subsequently diluted as needed in deionized water. Adsorption experiments were carried out by mixing samples and 20 mL synthesized wastewater in a 50 mL conical for 120 min with stirring at 250 rpm (adsorption kinetics excluded). The solution pH was adjusted as needed using 0.1 M HCl and 0.1 M NaOH solutions.

The kinetic experiments were performed in the solution with a Pb(II) concentration of 100 mg L⁻¹, a control adsorption time of 1,400 min, and a pH of 5. The adsorption isotherms were carried out in a series of solutions with different initial Pb(II) concentrations (100–700 mg L⁻¹). At the end of every experiment, the collected sample was separated from the solid adsorbent with 0.45 μm disposable microporous membrane filters. In order to evaluate the regeneration potential and reusability of ARWF, the performance of ARWF was studied through four successive experimental cycles. The spent adsorbent was collected and then regenerated using HCl solution (0.1 mol L⁻¹) with stirring for 60 min. The regenerated adsorbent was washed with deionized water until the pH was neutralized and then dried for the next Pb(II) adsorption experiment. The concentrations of Pb(II) ions were measured using an atomic absorption spectrometer (AAS, Varian SpectrAA220). The adsorption volume and removal rates were calculated according to the following formulas:

$$q_e = \frac{(C_0 - C_e) \times V}{m} \quad (1)$$

$$R = \frac{(C_0 - C_e)}{C_0} \times 100\% \quad (2)$$

where C_0 (mg L⁻¹) and C_e (mg L⁻¹) are the initial and equilibrium concentrations of the Pb(II) solution, respectively; q_e (mg g⁻¹) is the adsorption capacity of saturation; V (L) and m (g) are the volumes of the solution and the mass of the samples, respectively; R (%) is the removal efficiency. Three samples were run in parallel for all treatment conditions, and the mean values ± standard deviation values were calculated.

3. Results and discussion

3.1. Characterization of the adsorbent

The surface morphology and the chemical distribution of ARWF (iron oxide supported acid-modified rock wool) was determined via SEM-EDS. As seen in Figs. 1a, d and g, the RW composed of large amounts of longitudinally interlaced fibers with a clean surface and a diametric range of about 5–10 μm. The porosity of RW is 96.9%, and this

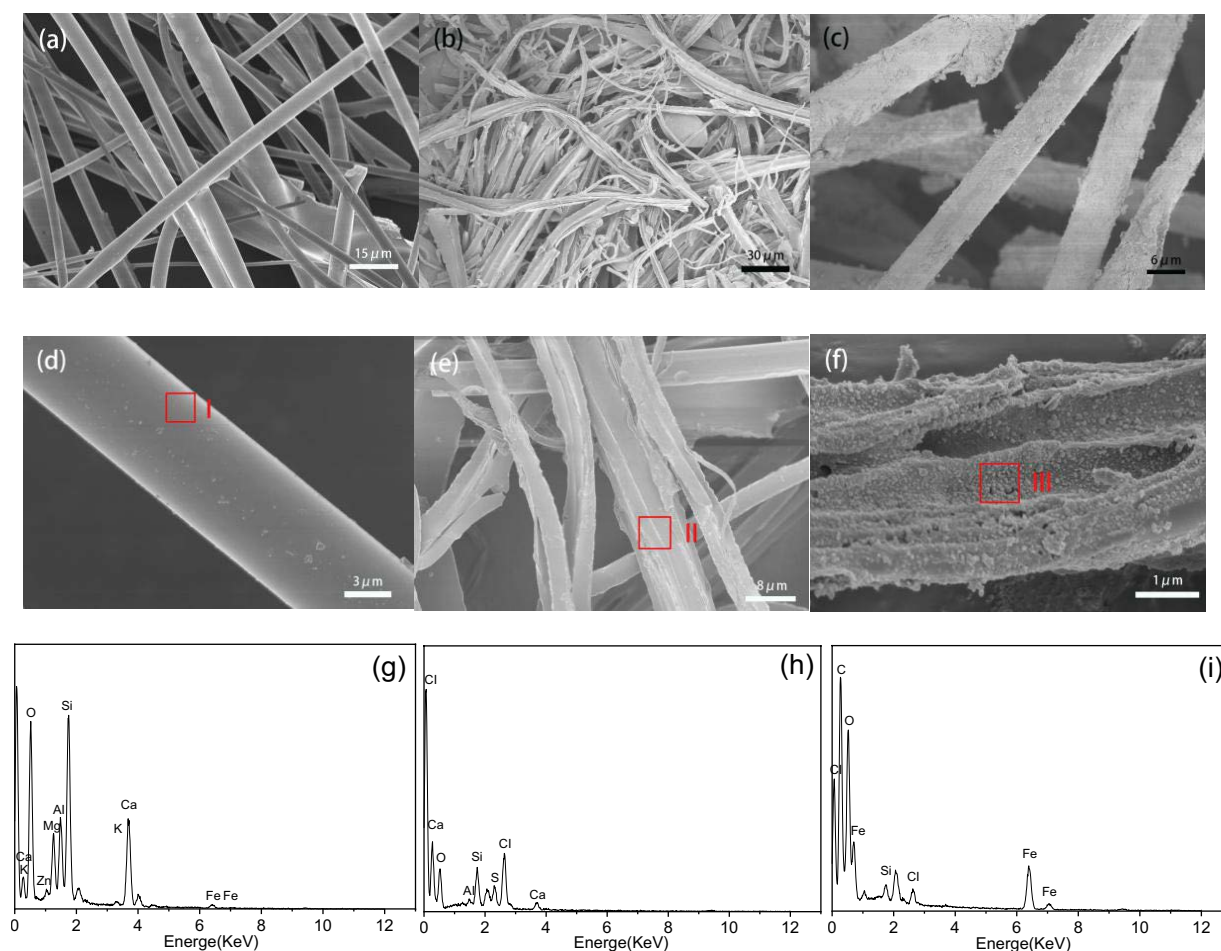


Fig. 1. Scanning electron microscopy images of (a and d) waste rock wool (RW), (b and e) acid-modified waste rock wool (ARW), and (c and f) acid-modified waste rock wool fiber (ARWF); (g–i) EDX spectra of waste RW (region I), ARW (region II), and ARWF (region III), respectively.

porous structure indicates potential as an adsorbent [21]. After pretreatment with 1.0 M HCl solution, a large number of micro-nano-cracks appeared on the fiber surface of the ARW, which provided the ARW with more active functional groups and a larger specific surface area than RW (Figs. 1b and e). More importantly, the rough surface of the fibers provided greater space for loading iron oxide nanoparticles and promoted dispersion of the nanoparticles via steric hindrance (Figs. 1c and f). As shown in Figs. 1f and i, a large number of precipitated particles appeared in the cracks on the surface of the ARW fibers, which were further confirmed by EDS elemental mapping to contain a large amount of iron; it can, therefore, be inferred that iron oxide nanoparticles were loaded onto the ARW surface. Furthermore, the addition of iron oxide particles improved the ARW's ability to adsorb Pb(II) and increased its specific surface area.

The crystallographic phases of the samples were investigated by XRD. As shown in Fig. 2a, the diffraction peak ($2\theta = 23.0^\circ$) in the XRD pattern of RW indicates that $\text{SiO}_2\text{-Al}_2\text{O}_3\text{-CaO-MgO}$ is the main component; the XRD pattern of ARW also carries a prominent peak at $2\theta = 21.0^\circ$, suggesting the presence of amorphous silica [22]. Diffraction peaks at $2\theta = 30.0^\circ, 35.5^\circ, 43.2^\circ, 53.5^\circ, 57.0^\circ, 62.6^\circ$ were also observed in the XRD pattern of ARWF, respectively, corresponding to reflections of (220), (311), (400), (422), (511) and (440) crystal planes of cubic phase of Fe_3O_4 [23], indicating the main component of the particles loaded onto the ARW is Fe_3O_4 . These findings were consistent with the analysis of EDX (Fig. 1i).

Active groups and chemical interactions in the ARWF system were evaluated by FTIR. As displayed in Fig. 2b, the characteristic peaks of 3413 and $1,019\text{ cm}^{-1}$ in the RW correspond to the tensile vibration of -OH and Si-O-Si , respectively. Following treatment with HCl solution (1.0 M), the absorption peak at $1,019\text{ cm}^{-1}$ disappeared, indicating that silicon oxide in ARW can be removed. Treatment with HCl also remarkably enhanced peaks at $3,396; 1,643,$ and $1,149\text{ cm}^{-1}$, indicating that HCl treatment can enrich -OH and -COOH groups in RW [24]. A new peak corresponding to Fe-O tensile vibration also emerged in the ARWF spectrum

at 562 cm^{-1} , and this was similar to the infrared band values of Fe_3O_4 reported in the literature. This indicates that Fe_3O_4 was incorporated successfully on the ARW surface. The peak located at $1,122\text{ cm}^{-1}$ might be caused by weak stretching of OH in goethite ($\alpha\text{-FeOOH}$) and lepidocrocite ($\gamma\text{-FeOOH}$) [25].

3.2. Removal efficiency of Pb(II) from water by different samples

In order to determine the optimal medium for lead removal, the abilities of RW, ARW, and ARWF were quantified to adsorb Pb(II) from aqueous solution. As shown in Fig. 3, the lead removal efficiency for all samples tested increased with time. RW was not efficient for Pb(II) removal (20%), whereas ARW performed slightly better than RW (23%), demonstrating that HCl treatment had a positive impact on RW's lead removal efficiency. This increased efficiency was mainly due to the improvements in porosity and surface functional groups provided by HCl treatment [24]. Furthermore, the ARWF displayed a better adsorption performance than ARW and Fe_3O_4 , mainly because Fe_3O_4 improved the adsorption capacity of ARW, and ARW prevented aggregation of Fe_3O_4 nanoparticles [26]. The adsorption of Pb(II) by three different ratios of ARWF was rapidly completed within 30 min. As the mass ratio of Fe_3O_4 increased, removal efficiency also increased notably. ARWF in mass ratios of 1:1 and 1:2 resulted in maximum removal efficiency (96.6% and 95.9%, respectively) within 30 min. Due to this optimal efficiency and economic considerations, ARWF with a mass ratio of ARW:Fe = 1:1 was chosen as the optimized sample for adsorption of Pb(II).

3.3. Effect of pH

It is well established that pH is the most critical factor affecting adsorption processes [26]. The chemistry of the surface functional groups of the adsorbed material can change with the pH of the solution, thus affecting the adsorption capacity of the material [39]. Hence, experiments were carried out in the pH range of 1–8 in order to determine the optimal pH for adsorption. As shown in Fig. 4, the initial

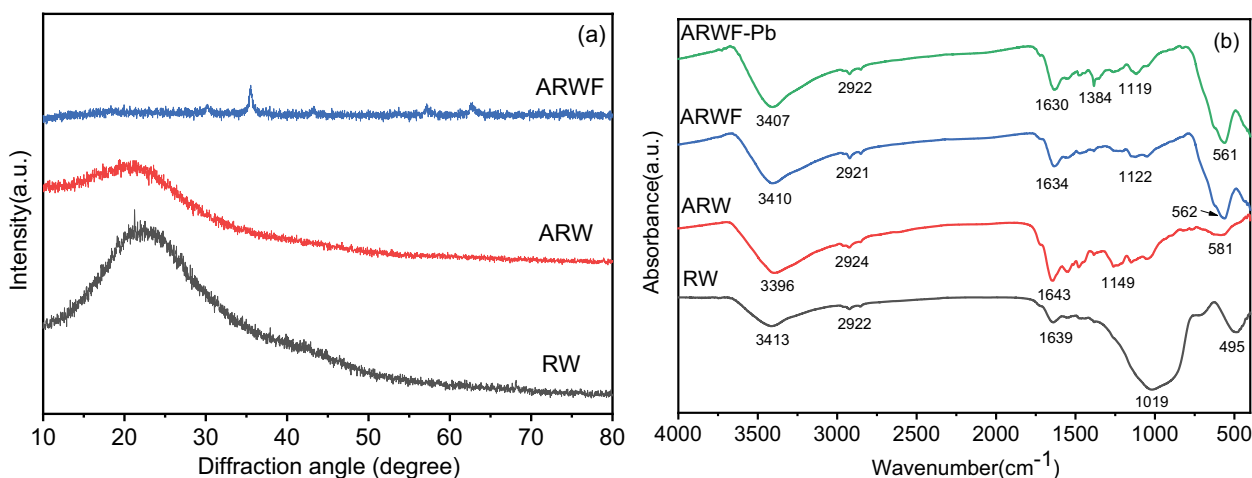


Fig. 2. X-ray diffraction patterns and Fourier transforms infrared spectroscopy spectra of rock wool, acid-modified waste rock wool, acid-modified waste rock wool fiber.

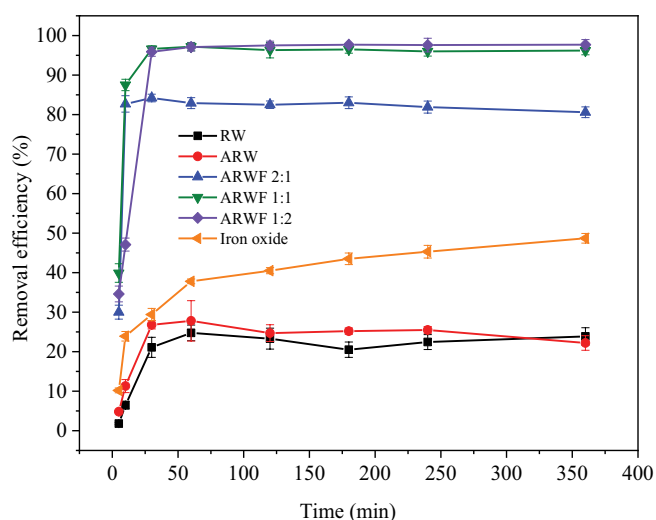


Fig. 3. Removal efficiency of Pb(II) from water by rock wool, acid-modified waste rock wool, iron oxide, and acid-modified waste rock wool fiber with different proportions.

pH value of the solution had a remarkable impact on the adsorption efficiency of ARWF. The adsorption capacity and removal efficiency of Pb(II) all increased markedly with increasing pH from 1 to 4 but did not increase with further increases in pH. At low pH, most of the adsorption sites on the ARWF surface were occupied by protons, making it difficult to adsorb Pb(II) ions from the solution because of the electrostatic repulsion force [37]. A high pH was conducive to the deprotonation of the sorbent surface, causing a reduction in ARWF's adsorption capacity [13]. Additionally, lead hydroxide precipitated above pH 7, and this negatively affected adsorption. Therefore, we chose to carry out subsequent adsorption experiments at pH 5. Under these conditions, the adsorption capacity and removal rate of ARWF for Pb(II) reached 49.9 mg g^{-1} and 99.45%, respectively.

3.4. Effect of adsorbent dosage

In order to determine the optimal dosage of ARWF, the effect of different doses was investigated while keeping other parameters constant. As demonstrated in Fig. 5, as the dosage of adsorbent increased in the range of $0.5\text{--}8 \text{ g L}^{-1}$, the unit adsorption of ARWF gradually reduced from 100 to 12.5 mg g^{-1} . This occurred mainly because there were fewer available adsorption sites at lower doses of ARWF and Pb(II) ions were in excess, so there were Pb(II) ions available for ARWF to adsorb, resulting in increased adsorption with increased ARWF. On the other hand, as ARWF dosage further increased, there were fewer Pb(II) ions available to adsorb, causing a reduction in unit adsorption capacity. As the dosage of ARWF increased, the removal efficiency of ARWF to Pb(II) gradually increased. When the dosage was increased to 2 g L^{-1} , the removal rate of Pb(II) increased faster because the active site of ARWF was not yet saturated, allowing for easy adsorption of Pb(II). This also weakened the competition between Pb(II) and H^+ , thus enhancing the chance of collision between ARWF and Pb(II) [27]. At a dosage of 2 g L^{-1} , we observed an adsorption

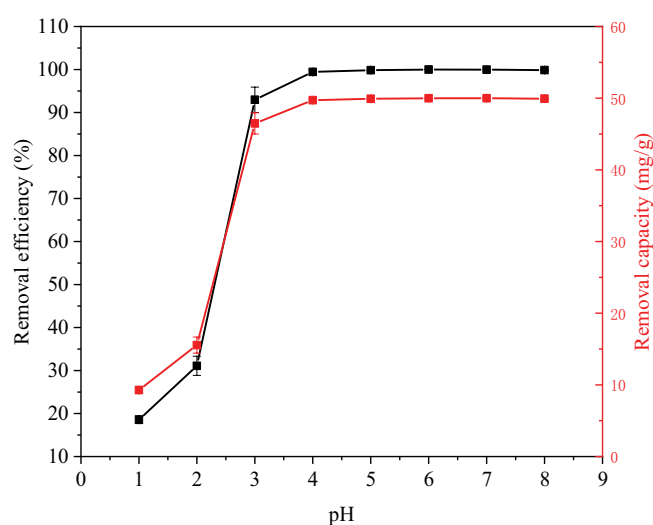


Fig. 4. Effect of pH on Pb(II) adsorption onto acid-modified waste rock wool fiber.

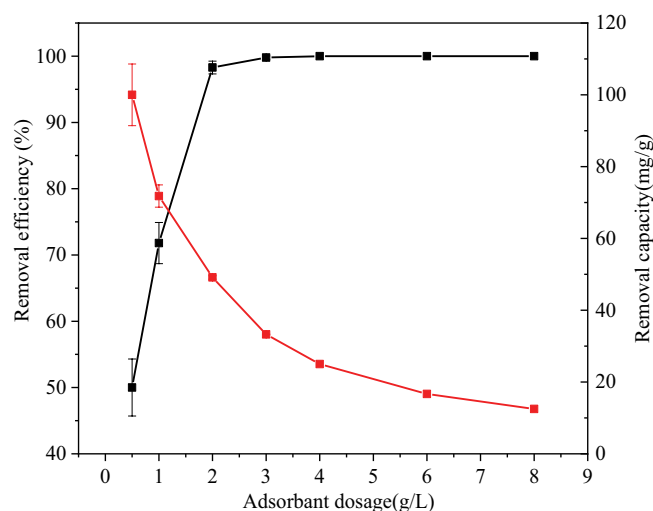


Fig. 5. Effect of adsorbent dosage on Pb(II) adsorption onto acid-modified waste rock wool fiber.

rate of 98.3%. Based on these results, 2 g L^{-1} was determined as the optimal dosage due to relatively high removal efficiency and unit adsorption capacity of ARWF for Pb(II).

3.5. Effect of initial Pb(II) concentration

As shown in Fig. 6, the adsorption effect of ARWF changed remarkably with different initial lead concentrations. When the initial concentration was between 50 and 150 mg L^{-1} , the removal rate of lead (II) stayed constant at around 99.9%. At initial concentrations above 150 mg L^{-1} , the removal rate gradually decreases with increased starting concentration. At low initial Pb(II) concentrations, the number of Pb(II) ions in solution was insignificant compared with the number of adsorption sites on the ARWF surface; therefore, the removal efficiency under these conditions was not very dependent on

the initial Pb(II) concentration [28]. The adsorption capacity of ARWF increased slowly with increased initial Pb(II) concentration, and as the initial concentration of Pb(II) increased to 600 mg L⁻¹, the removal capacity of ARWF increased to 111.3 mg L⁻¹. One possible explanation for

this is that the rate of Pb(II) ions passing from the solution to the adsorbent surface and the mass transfer driving force of the solution increased with increased Pb(II) ions concentration, thus increasing the probability of contact between ARWF and Pb(II) ions. As the initial concentration was further increased, the surface-active sites of ARWF were entirely occupied by Pb(II), and the loading capacity reached saturation [29].

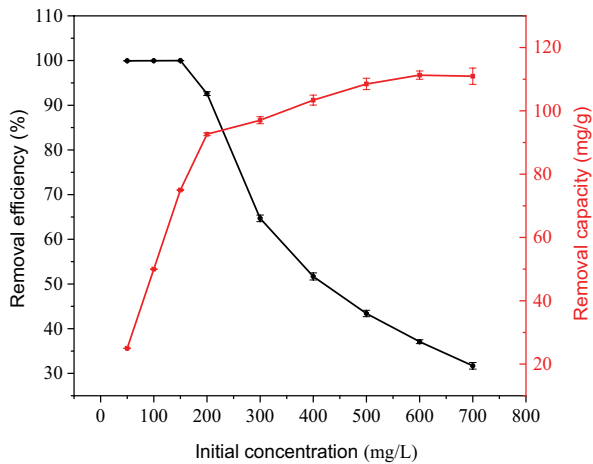


Fig. 6. Effect of initial concentration on Pb(II) adsorption onto acid-modified waste rock wool fiber.

3.6. Adsorption kinetics and isotherms of lead

Fig. 7a shows the kinetics curve for the adsorption of ARWF to Pb(II) ions with time. The adsorption of Pb(II) by ARWF occurred quickly within the first 180 min, then slowed down and finally reached equilibrium. This was mainly due to the low relative concentration of Pb(II) ions during the initial stage of adsorption, which allowed the Pb(II) ions to bind rapidly to the surface active sites of the ARWF. As the adsorption reaction progressed, more and more Pb(II) ions were adsorbed onto the ARWF surface, resulting in occupation of the adsorbent sites and an increase in repulsion between Pb(II) ions in solution and on the adsorbent surface. The adsorption experiment results were fitted using pseudo-first-order (3), pseudo-second-order (4), and intra-particle diffusion models (5), respectively.

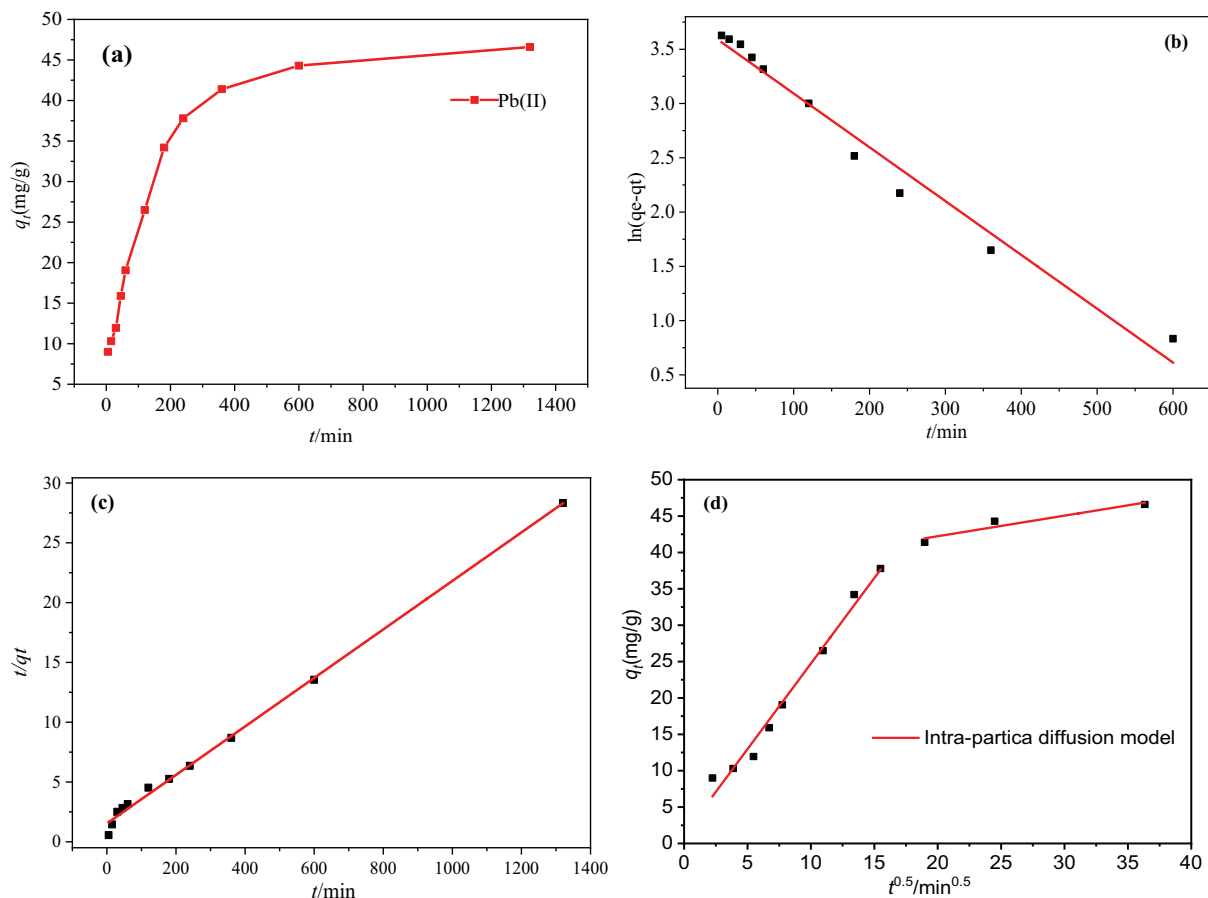


Fig. 7. Kinetics of Pb(II) adsorption onto acid-modified waste rock wool fiber (a) and pseudo-first-order (b), pseudo-second-order (c) and intra-particle diffusion (d) plot for adsorption.

$$\ln(q_e - q_t) = \ln q_e - k_1 t \quad (3)$$

$$\frac{t}{q_t} = \frac{1}{(k_2 q_e^2)} + \frac{t}{q_e} \quad (4)$$

$$q_t = k_d t^{1/2} + C \quad (5)$$

where q_e (mg g⁻¹) and q_t (mg g⁻¹), respectively, represent the adsorption capacity at equilibrium time and t time; k_1 (min⁻¹) and k_2 (g mg⁻¹ min⁻¹) represent adsorption rate constants of pseudo-first-order and pseudo-second-order, respectively; k_d was the rate constant of intra-particle diffusion.

Figs. 7b–d display adsorption kinetic curves fitted by the three models. The model fitting parameters are shown in Table 1. As shown in Table 1 and Fig. 7, the correlation coefficient (R^2) of the pseudo-second-order kinetics was 0.996, which was higher than the R^2 value (0.975) fitted by the pseudo-first-order kinetics equation, although both models could fit the sorption data well. The pseudo-second-order kinetics model was more suitable for describing the adsorption behavior of ARWF to Pb(II). The adsorption process is based on chemical adsorption, and the equilibrium adsorption capacity (q_e) calculated from the fitted model was consistent with the actual results [30].

In order to further understand each stage of adsorption process control, the adsorption data were fitted and analyzed using the intra-particle diffusion model (Fig. 7d). As displayed in Fig. 7d, the adsorption process included two stages. The first stage (0–240 min) was a surface reaction process with a rapid increase in adsorption capacity, which was more consistent with the intra-particle diffusion model ($R^2 = 0.983$). In the initial phase of the reaction, the surface of ARWF had plenty of adsorption sites and could bind to sufficient Pb(II) ions. In the second stage (240 min – adsorption balance), the reaction rate tended to be slow, and adsorption gradually reached saturation as Pb(II) gradually diffused into the micropores of ARWF. Additionally, the fitted straight line of the two stages did not go through the origin, indicating that the intra-particle diffusion was not the single rate control step in the adsorption of Pb(II) by ARWF, which also involved liquid film diffusion and surface adsorption [31].

To evaluate the adsorption performance of ARWF on Pb(II), an adsorption isotherm experimental study was performed. The Langmuir and Freundlich adsorption isotherm models were the common mathematical models used to describe the equilibrium relationship. Eqs. (6) and (7) indicate the Langmuir and the Freundlich isotherm models, respectively.

$$q_e = \frac{q_m \cdot k_L \cdot C_e}{1 + k_L \cdot C_e} \quad (6)$$

$$q_e = k_F \cdot C_e^{1/n} \quad (7)$$

In the formula, C_e (mg L⁻¹) is the concentration of Pb(II) in solution at adsorption equilibrium; q_e (mg g⁻¹) and q_m (mg g⁻¹) are the adsorption capacity at adsorption equilibrium and the maximum adsorption capacity of the sorbent, respectively; k_L (L mg⁻¹) and k_F (mg/g)·(1/mg)^{1/n} are constants related to thermodynamics and adsorption strength, respectively. The constant n correlates with the adsorption ability. The parameter R_L can be calculated by using the k_L value, which is used to determine the type of Langmuir isotherm and defined by Eq. (8).

$$R_L = \frac{1}{1 + k_L C_0} \quad (8)$$

where C_0 (mg L⁻¹) is the metal ion concentration.

The adsorption isotherms were conducted at temperatures of 278, 288, 298 K with initial concentrations of Pb(II) ions of 50–800 mg L⁻¹. The adsorption isotherm of ARWF on Pb(II) and model fitting results under these conditions are illustrated in Fig. 8 and Table 2, respectively. The adsorption capacity of Pb(II) gradually increased with increasing Pb(II) equilibrium concentration in solution. The fitting of the data to the Langmuir isotherm model ($R^2 = 0.9689$ – 0.9792) was more accurate than the Freundlich isothermal model ($R^2 = 0.6567$ – 0.7670) at different temperatures. The Langmuir model was more able to describe the adsorption process of ARWF on Pb(II). Notably, the Langmuir model describes the equivalent adsorption and adsorbent surfaces at all sites that were monolayer covered [32]. Specifically, R_L (Langmuir model) values obtained were between 0 and 1, indicating that the adsorption of Pb(II) ions in solution by ARWF was favorable [33]. The results indicate that ARWF has excellent adsorption ability for lead in water. The maximum adsorption capacity of ARWF for Pb(II) at 298 K, calculated by Langmuir's equation was 123.15 mg g⁻¹, which is higher than previously reported in the literature (Table 3). The results indicate that ARWF has high adsorption efficiency and fast adsorption speed, making it a promising adsorption material for lead removal from water.

3.7. Regeneration and reusability

When evaluating an adsorbent, it is important not to examine only adsorption capacity but also potential for

Table 1
Adsorption kinetic model and fitting parameters of ARWF for Pb(II)

Pseudo-first-order			Pseudo-second-order			Intra-particle diffusion			
						Initial stage		Second stage	
Q_e (mg g ⁻¹)	k_1 (min ⁻¹)	R^2	Q_e (mg g ⁻¹)	k_2 (g mg ⁻¹ min ⁻¹)	R^2	k_d	R^2	k_d	R^2
36.18	0.0050	0.975	49.31	0.0003	0.996	2.3514	0.983	0.2829	0.927

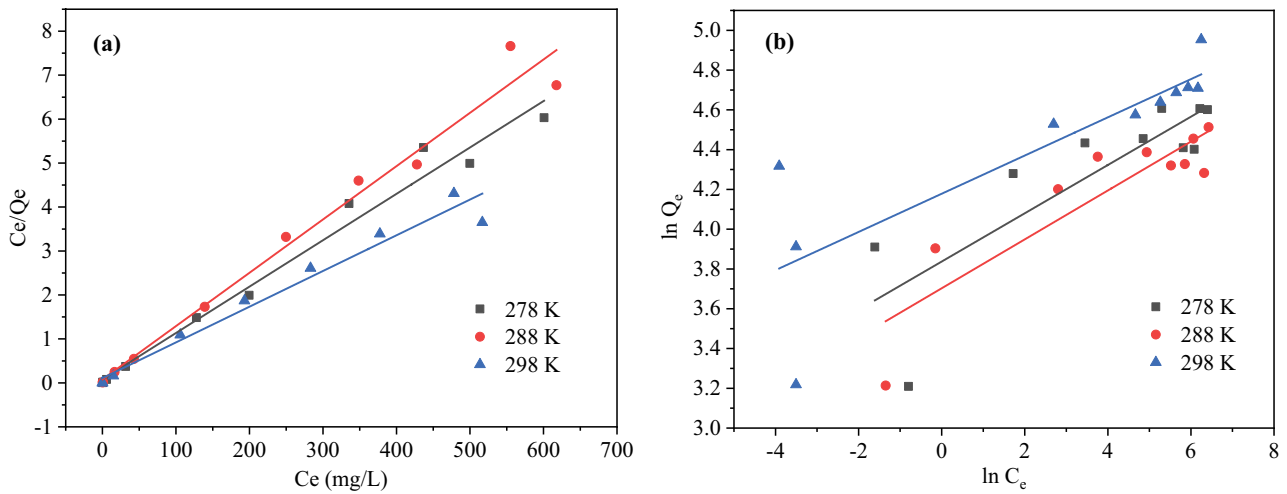


Fig. 8. Langmuir (a) and Freundlich (b) isotherm models for adsorption of Pb(II) by ARWF at different temperatures.

Table 2
Fitting parameters of isotherm model for ARWF adsorption of Pb(II)

T (K)	Langmuir				Freundlich		
	k_L (L mg ⁻¹)	q_m (mg g ⁻¹)	R_L	R^2	k_f (mg/g)·(1/mg) ^{1/n}	n	R^2
278	0.1329	94.79	0.009–0.131	0.9792	46.40	8.2379	0.6628
288	0.1546	82.44	0.008–0.115	0.9762	65.25	8.1340	0.7670
298	0.0750	123.15	0.016–0.211	0.9689	42.07	10.4102	0.6567

Table 3
Adsorption capacities of adsorbents reported in the literature for Pb(II)

Adsorbent	T (°C)	Maximum capacity (mg g ⁻¹)	pH	Reference
Modified cotton	20	69.5	–	[40]
Biochar from maple wood	25	43.3	–	[7]
Pigeon peas hulls	20	20.83	4.0	[41]
Bamboo charcoal modified with KMnO ₄	25	55.56	5.0	[42]
<i>Pleurotus ostreatus</i> immobilized iron oxide	–	32.1	5.0	[43]
β-Cyclodextrin modified biochar	35	240.13	5.5	[44]
APTES functionalized magnetic biochar	–	64.92	–	[45]
ARWF	25	123.15	5.0	This study

regeneration and reusability. Accordingly, four successive adsorption regeneration cycle experiments were performed to examine the regeneration performance of ARWF. As shown in Fig. 9, the removal efficiency of ARWF on Pb(II) was maintained at above 80% in four regeneration cycles. Therefore, this sorbent has promising application for Pb-wastewater treatment.

3.8. Adsorption mechanism analysis

Based on the impact factor analysis, SEM-EDS, XRD, FTIR, adsorption kinetics, adsorption isotherm, and the adsorption mechanism of aqueous Pb(II) by ARWF were

investigated. Fe₃O₄ loaded onto ARW played a pivotal role in removing Pb(II) from water, and ARW fibers were responsible for supporting and dispersing Fe₃O₄ nanoparticles. The solution pH impacted the removal efficiency of Pb(II), which demonstrates electrostatic attraction between ARWF and Pb(II) ions. The surface of ARWF adsorbent may undergo a protonation–deprotonation reaction [13]. The number of positively charged sites gradually increases as the pH of the solution decreases. Positive charges on the ARWF surface are not favorable for Pb(II) adsorption due to electrostatic repulsion. Moreover, at lower pH conditions, excess protons compete with Pb(II) ions for sorption position, resulting in reduced adsorption ability of

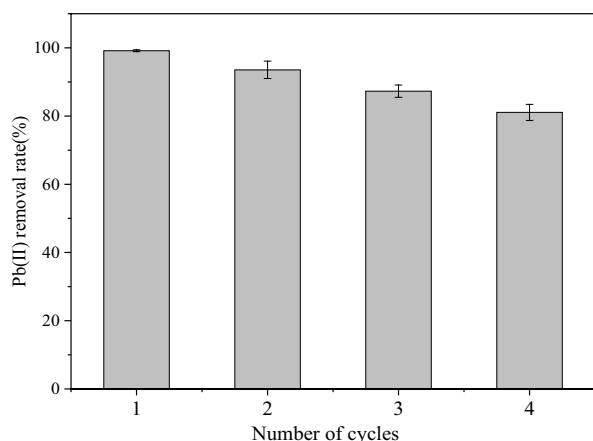


Fig. 9. Regeneration study of the acid-modified waste rock wool fiber. Experiment conditions: adsorbent dosage = 2 g L⁻¹; pH = 5.0; T = 25°C ± 1°C.

the ARWF [26]. Therefore, the electrostatic effect on the ARWF surface may be an essential mechanism of adsorption. Additionally, changes in pH not only affect the surface charge and ionization degree but also determine the form of lead present in the solution. The presence of Pb(II) ions in the forms of Pb(OH)⁺, Pb²⁺, Pb(OH)₂, and Pb(OH)₄²⁺ at different pH values led to differences in the performance of adsorbents. When pH is greater than 6.5, Pb(OH)₂ is the primary form of lead in the solution, whereas when pH is less than 6.5, the primary forms are Pb²⁺ and Pb(OH) [34].

The pseudo-first-order, pseudo-second-order kinetic models and Langmuir isothermal adsorption models fit the experimental results, indicating that ARWF adsorbed Pb(II) effectively. The chemical adsorption mechanism was crucial, and the adsorption process was similar to monolayer adsorption [35]. FTIR detection results showed that the surface of ARWF contained large amounts of –COOH and –OH functional groups. Upon binding of Pb(II), the characteristic peaks associated with these groups mostly shifted; this probably occurred due to ion exchange of Pb(II) with protons in –OH and –COOH or direct complexation of oxygen-containing groups with Pb(II) [36,38]. Hence, ion exchange and functional group complexation may also be significant mechanisms that affect adsorption. On all counts, the adsorption of Pb(II) by ARWF is a complex process that occurs through the joint action of various mechanisms involving a combination of physical and chemical interactions, including surface complexation, ion exchange, and electrostatic attraction.

4. Conclusion

In this study, waste RW was examined as a solution to the problems of agglomeration and separation of iron oxide in the removal of Pb(II) from water. The SEM results show that the surface of RW fibers treated with HCl contained large amounts of micro-nano-cracking and iron oxide nanoparticles which were distributed uniformly on the surface of ARW. The large specific surface area of the ARW reinforced the dispersion of iron oxide, producing more adsorption sites for the removal of Pb(II). Furthermore, XRD analyses revealed that the major constituent of the generated

particles was Fe₃O₄. Due to the porous structure of ARWF, 99.45% Pb(II) adsorption was achieved in only 30 min, and adsorption capacity of 123.15 mg g⁻¹ could be reached at pH 4–8. Based on adsorption kinetics and isotherm studies, the adsorption of Pb(II) on ARWF was consistent with pseudo-second-order and Langmuir models. ARWF was demonstrated to have good potential for regeneration and reuse after four consecutive cycles. The superior Pb(II) adsorption capacity and excellent regeneration and reuse potential of ARWF indicate that this adsorbent has broad prospects for practical application in Pb-contaminated water treatment.

Acknowledgments

The authors thank Mr. Chunhao Liang and Mr. Chaoqun Zhang for their assistance with the technical aspects of this laboratory work and acknowledge the Liaoning Academy of Agricultural Sciences for providing test facilities.

References

- [1] H. Salih, S. Musaad, C. Patterson, G. Sorial, M. Schock, Lead adsorption into activated carbon: a critical review of the literature, *Adv. Environ. Res.*, 34 (2014) 1–24.
- [2] Y. Liu, Z.C. Liu, J. Gao, J.D. Dai, J. Han, Y. Wang, J.M. Xie, Y.S. Yan, Selective adsorption behavior of Pb(II) by mesoporous silica SBA-15-supported Pb(II)-imprinted polymer based on surface molecularly imprinting technique, *J. Hazard. Mater.*, 186 (2011) 197–205.
- [3] J.X. Yu, L.Y. Wang, R. Chi, Y.F. Zhang, Z.G. Xu, J. Guo, Removal of cationic dyes: basic magenta and methylene blue from aqueous solution by adsorption on modified loofah, *Res. Chem. Intermed.*, 39 (2013) 3775–3790.
- [4] C. Ribeiro, F.B. Scheufele, F.R. Espinoza-Quiñones, A.N. Módenes, M.G. Adeodato Vieira, A.D. Kroumou, C.E. Borba, A comprehensive evaluation of heavy metals removal from battery industry wastewaters by applying bio-residue, mineral and commercial adsorbent materials, *J. Mater. Sci.*, 53 (2018) 7976–7995.
- [5] A. Bhattacharya, S.N. Naik, S.K. Khare, Harnessing the biomineralization ability of urease producing *Serratia marcescens* and *Enterobacter cloacae* EMB19 for remediation of heavy metal cadmium (II), *J. Environ. Manage.*, 215 (2018) 143–152.
- [6] C.H. Chen, Y.S. Lin, S.J. Wu, F.L. Mi, Multifunctional nanoparticles prepared from arginine-modified chitosan and thiolated fucoidan for oral delivery of hydrophobic and hydrophilic drugs, *Carbohydr. Polym.*, 193 (2018) 163–172.
- [7] Q. Wang, B. Wang, X.Q. Lee, J. Lehmann, B. Gao, Sorption and desorption of Pb(II) to biochar as affected by oxidation and pH, *Sci. Total. Environ.*, 634 (2018) 188–194.
- [8] K. Ranganathan, Adsorption of Hg(II) ions from aqueous chloride solutions using powdered activated carbons, *Carbon*, 41 (2003) 1087–1092.
- [9] S.V. Mohan, J. Karthikeyan, Removal of lignin and tannin colour from aqueous solution by adsorption onto activated charcoal, *Environ. Pollut.*, 97 (1997) 183–197.
- [10] A. Kausar, G. Mackinnon, A. Alharthi, J. Hargreaves, M. Iqbal, A green approach for the removal of Sr(II) from aqueous media: kinetics, isotherms and thermodynamic studies, *J. Mol. Liq.*, 257 (2018) 164–172.
- [11] A. Rashid, H.N. Bhatti, M. Iqbal, S. Noreen, Fungal biomass composite with bentonite efficiency for nickel and zinc adsorption: a mechanistic study, *Ecol. Eng.*, 91 (2016) 459–471.
- [12] A. Kausar, H.N. Bhatti, G. Mackinnon, Re-use of agricultural wastes for the removal and recovery of Zr(IV) from aqueous solutions, *J. Taiwan Inst. Chem. Eng.*, 59 (2016) 330–340.
- [13] Nashaat N. Nassar, Rapid removal and recovery of Pb(II) from wastewater by magnetic nano-adsorbents, *J. Hazard. Mater.*, 184 (2010) 538–546.

- [14] A. Cheng, W.T. Lin, R. Huang, Application of rock wool waste in cement-based composites, *Mater. Des.*, 32 (2011) 636–642.
- [15] M. Jirickova, R. Cerny, Effect of hydrophilic admixtures on moisture and heat transport and storage parameters of mineral wool, *Construct. Build. Mater.*, 20 (2006) 425–434.
- [16] M.M. Galera, E. Cho, E. Tuuguu, S.J. Park, D.M. Farnazo, C. Jee, N.J. Yoo, W.J. Chung, Removal of NH_3 , H_2S and toluene by biofilters packed with rock wool/compost media, *J. Ind. Eng. Chem.*, 13 (2007) 895–902.
- [17] V.W.Y. Tam, W.S. Lu, Construction waste management profiles, practices, and performance: a cross-jurisdictional analysis in four countries, *Sustainability*, 8 (2016) 190.
- [18] V.W.Y. Tam, C.M. Tam, A review on the viable technology for construction waste recycling, *Resour. Conserv. Recycl.*, 47 (2016) 209–221.
- [19] O. Väntsi, T. Kärki, Mineral wool waste in Europe: a review of mineral wool waste quantity, quality, and current recycling methods, *J. Mater. Cycles Waste Manage.*, 16 (2014) 62–72.
- [20] Y.F. Shen, J. Tang, Z.H. Nie, Y.D. Wang, Y. Ren, L. Zuo, Preparation and application of magnetic Fe_3O_4 nanoparticles for wastewater purification, *Sep. Purif. Technol.*, 68 (2009) 312–319.
- [21] T. Zhang, L. Kong, Y. Dai, X. Yue, J. Rong, F. Qiu, J. Pan, Enhanced oil and organic solvents absorption by polyurethane foams composites modified with MnO_2 nanowires, *Chem. Eng. J.*, 309 (2017) 7–14.
- [22] J. Athinarayanan, V.S. Periasamy, M.A. Alsaif, A.A. Al-Warthan, A.A. Alshatwi, Presence of nanosilica (E551) in commercial food products: TNF-mediated oxidative stress and altered cell cycle progression in human lung fibroblast cells, *Cell Biol. Toxicol.*, 30 (2014) 89–100.
- [23] Z.H. Zhou, J. Wang, X. Liu, H.S.O. Chan, Synthesis of Fe_3O_4 nanoparticles from emulsions, *J. Mater. Chem.*, 11 (2011) 1704–1709.
- [24] L.L. Zhou, R.R. Li, G.L. Zhang, D.F. Wang, D.Q. Cai, Z.Y. Wu, Zero-valent iron nanoparticles supported by functionalized waste rock wool for efficient removal of hexavalent chromium, *Chem. Eng. J.*, 339 (2018) 85–96.
- [25] H.F. Zhou, R. Yi, J.H. Li, Y. Su, X.H. Liu, Microwave-assisted synthesis and characterization of hexagonal Fe_3O_4 nanoplates, *Solid State Sci.*, 12 (2010) 99–104.
- [26] Y.N. Zhu, Y.N. Jiang, Z.Q. Zhu, H. Deng, H. Ding, Y.H. Li, L.H. Zhang, J. Lin, Preparation of porous hydroxyapatite-carbon composite with the bio-template of sugarcane top stems and its use for the Pb(II) removal, *J. Cleaner Prod.*, 187 (2018) 650–661.
- [27] K. Fukushima, Turbulent pattern formation and diffusion in the early-time dynamics in the relativistic heavy-ion collision, *Phys. Rev. C*, 89 (2013) 167–176.
- [28] R.H. Zhu, R.B. Yu, J.X. Yao, D. Mao, C.J. Xing, D. Wang, Removal of Cd^{2+} from aqueous solutions by hydroxyapatite, *Catal. Today*, 139 (2008) 94–99.
- [29] X.S. Wang, L. Zhu, H.J. Lu, Surface chemical properties and adsorption of Cu(II) on nanoscale magnetite in aqueous solution, *Desalination*, 276 (2011) 154–160.
- [30] C. Li, Z.Q. Zhu, S. Cao, Y.N. Zhu, H. Ding, Adsorption characteristics of copper in water by the porous biomorphogenic composite of HAP/C with eucalyptus wood template, *Environ. Sci.*, 38 (2017) 1074–1083.
- [31] Y.B. Sun, C.C. Ding, W.C. Cheng, X.K. Wang, Simultaneous adsorption and reduction of U(VI) on reduced graphene oxide-supported nanoscale zerovalent iron, *J. Hazard. Mater.*, 280 (2014) 399–408.
- [32] F. Long, J.L. Gong, G.M. Zeng, Removal of phosphate from aqueous solution by magnetic Fe-Zr binary oxide, *Chem. Eng. J.*, 171 (2011) 448–455.
- [33] C. Jin, X.Y. Zhang, J.N. Xin, G.F. Liu, G.M. Wu, Z.W. Kong, J.W. Zhang, Clickable synthesis of 1,2,4-triazole modified lignin-based adsorbent for the selective removal of Cd(II), *ACS Sustainable Chem. Eng.*, 5 (2017) 4086–4093.
- [34] H. Chen, G.L. Dai, J. Zhao, A.G. Zhong, J.Y. Wu, H. Yan, Removal of copper(II) ions by a biosorbent-*Cinnamomum camphora* leaves powder, *J. Hazard. Mater.*, 177 (2010) 228–236.
- [35] T.K. Naiya, A.K. Bhattacharya, S.K. Das, Adsorption of Pb(II) by sawdust and neem bark from aqueous solutions, *Environ. Prog.*, 27 (2008) 313–328.
- [36] G. Vinodhkumar, J. Wilson, S.S.R. Inbanathan, I. Vetha Potheher, M. Ashokkumar, A.C. Peter, Solvothermal synthesis of magnetically separable reduced graphene oxide/ Fe_3O_4 hybrid nanocomposites with enhanced photocatalytic properties, *Phys. B*, 580 (2019) 411752.
- [37] Z.J. Yi, J. Yao, H.L. Chen, F. Wang, X. Liu, J.S. Xu, Equilibrium and kinetic studies on adsorption of Pb(II) by activated palm kernel husk carbon, *Desal. Water Treat.*, 57 (2016) 7245–7253.
- [38] J. Wei, Z. Wei, L. Liao, S. Zhao, D. Wang, Aqueous Pb(II) removal by adsorption on amine-functionalized mesoporous silica SBA-15, *Chin. J. Environ. Eng.*, 8 (2014) 1825–1830.
- [39] N. Jiang, Y. Xu, Y. Dai, W. Luo, L. Dai, Polyaniline nanofibers assembled on alginate microsphere for Cu^{2+} and Pb^{2+} uptake, *J. Hazard. Mater.*, 215–216 (2012) 17–24.
- [40] B. Gao, A.R. Zimmerman, Z.H. Ding, X. Hu, Sorption and cosorption of lead(II) and methylene blue on chemically modified biomass, *Bioresour. Technol.*, 167 (2014) 569–573.
- [41] D.K. Venkata Ramana, D. Harikishore Kumar Reddy, J.S. Yu, K. Seshaiiah, Pigeon peas hulls waste as potential adsorbent for removal of Pb(II) and Ni(II) from water, *Chem. Eng. J.*, 197 (2012) 24–33.
- [42] Y. Wang, X.J. Wang, X. Wang, M. Liu, L.Z. Yang, Z. Wu, S.Q. Xia, J.F. Zhao, Adsorption of Pb(II) in aqueous solutions by bamboo charcoal modified with KMnO_4 via microwave irradiation, *Colloid Surf. A*, 414 (2012) 1–8.
- [43] S. Özdemir, M.S. Yalcin, E. Kilinc, Preconcentrations of Ni(II) and Pb(II) from water and food samples by solid-phase extraction using *Pleurotus ostreatus* immobilized iron oxide nanoparticles, *Food Chem.*, 336 (2020) 127675.
- [44] J.H. Qu, M. Dong, S.Q. Wei, Q.J. Meng, L.M. Hu, Q. Hu, L. Wang, W. Han, Y. Zhang, Microwave-assisted one pot synthesis of β -cyclodextrin modified biochar for concurrent removal of Pb(II) and bisphenol A in water, *Carbohydr. Polym.*, 250 (2020) 117003.
- [45] E.C. Nnadozie, P.A. Ajibade, Adsorption, kinetic and mechanistic studies of Pb(II) and Cr(VI) ions using APTES functionalized magnetic biochar, *Microporous Mesoporous Mater.*, 309 (2020) 110573.